Scripta Materialia 167 (2019) 26–30

Contents lists available at ScienceDirect

Scripta Materialia

journal homepage: www.elsevier.com/locate/scriptamat

Feasible transformation of $MgCo_2O_4$ from spinel to defect rocksalt structure under electron irradiation

Norihiko L. Okamoto *, Kohei Shimokawa, Hiroshi Tanimura, Tetsu Ichitsubo *

Institute for Materials Research, Tohoku University, 2-1-1 Katahira, Aoba-ku, Sendai 980-8577, Japan

ARTICLE INFO

Article history:
Received 14 February 2019
Received in revised form 20 March 2019
Accepted 22 March 2019
Available online xxxx

Keywords:
Diffusion
Entropy
Irradiation effect
STEM HAADF
Nudged elastic band (NEB) method

ABSTRACT

Spinel $MgCo_2O_4$ oxide, expected as a cathode material candidate for magnesium rechargeable battery, undergoes spinel-to-rocksalt transition accompanied with Mg insertion. Upon scanning-transmission-electron-microscopy observation, cations located at the tetrahedral sites readily migrate to the adjacent octahedral sites due to electron irradiation (without any Mg insertion), so that the spinel structure changes to a defect rocksalt structure with cation disorder. This together with first-principles calculations demonstrates that there is little energetic preference for Mg cation between the tetrahedral and octahedral sites, accounting for the feasibility of the Mg insertion into the spinel $MgCo_2O_4$ cathode via intercalation and push-out process of Mg cation.

Lithium (Li) ion batteries have been used for portable electronic devices and electric vehicles because of their high energy density, rechargeability and cyclability. However, the energy density of the electrode materials is approaching their theoretical limit unless Li metal is used as the anode materials instead of the carbonaceous materials currently used. Li metal was once in a practical use as the anode material [1], but eventually failed because the notorious problem of the dendritic growth of Li metal upon charge [2] could not be solved. Therefore, in order to improve the energy density of rechargeable batteries, a new type of metal-anode battery system is required. As an alternative of Li metal-anode battery, magnesium (Mg) metal-anode battery, in which the dendritic growth of Mg tends to be suppressed [3–5], have attracted much attention owing to their potential to more safely store energy at lower cost and volume than the conventional Li ion batteries [6,7]. In the advancing research field of Mg rechargeable batteries, however, it has been difficult to find out suitable cathode materials that simultaneously exhibit high electromotive force and high cation mobility [8,9]. For example, the Chevrel-type sulfides such as Mo_6S_8 can operate at ambient temperature because of high cation mobility, although the electromotive force is as low as 1.0–1.2 V [10,11]. On the other hand, oxide-based cathode materials exhibits high electromotive force although the cation mobility is poor due to their high activation energy of diffusion [12].

However, our research group has recently found that Mg insertion and extraction can occur in some spinel oxides ($MgCo_2O_4$, $MgMn_2O_4$, and Co_3O_4), which is facilitated by slightly elevating temperature (100–150 °C) [13]. In case of spinel $MgCo_2O_4$, Mg insertion occurs at a significantly high potential of about 2.9 V vs. Mg^{2+}/Mg, and its capacity approximately amounts to 200 mAh g^{-1} (theoretically 260 mAh g^{-1}) [13]. We have substantiated an eccentric mechanism on Mg insertion into spinel-oxide lattices, termed “intercalation and push-out” process [13]. This Mg insertion into a spinel structure occurs via dual-phase reaction of the spinel ($MgCo_2O_4$) and rocksalt ($Mg_2Co_2O_4$) phases [13]. As shown in Figs. 1(a) and 1(b), the atomic sites in the spinel structure with the space group of $Fd\bar{3}m$ are generally denoted as 8*a*, 16*d* (cation sites), and 32*e* (oxygen sites) in the Wyckoff notation while those in the rocksalt structure are denoted as 16*c*, 16*d* (cation sites) and 32*e* (oxygen sites) when assigned to the same space group; incidentally, the cation and oxygen sites respectively are actually denoted as 4*a* and 4*b* sites when assigned to the genuine space group of $Fm\bar{3}m$. Thus, a spinel structure can be regarded as a rocksalt-like structure whose octahedral 16*c* sites are vacant and instead the tetrahedral 8*a* sites are occupied by cations. Therefore, it is expected that upon Mg intercalation Mg cations are inserted into 16*c* vacant sites in the spinel lattice and are pushing out the cations originally located at the 8*a* sites to the 16*c* sites, eventually to form a rocksalt structure [13]. The viability of the Mg insertion in the spinel $MgCo_2O_4$ suggests that cation migration from the 8*a* to 16*c* sites readily occurs in order to accommodate the inserted Mg cation,

* Corresponding authors.
E-mail addresses: nlokamoto@imr.tohoku.ac.jp (N.L. Okamoto), tichi@imr.tohoku.ac.jp (T. Ichitsubo).

https://doi.org/10.1016/j.scriptamat.2019.03.034
1359-6462/

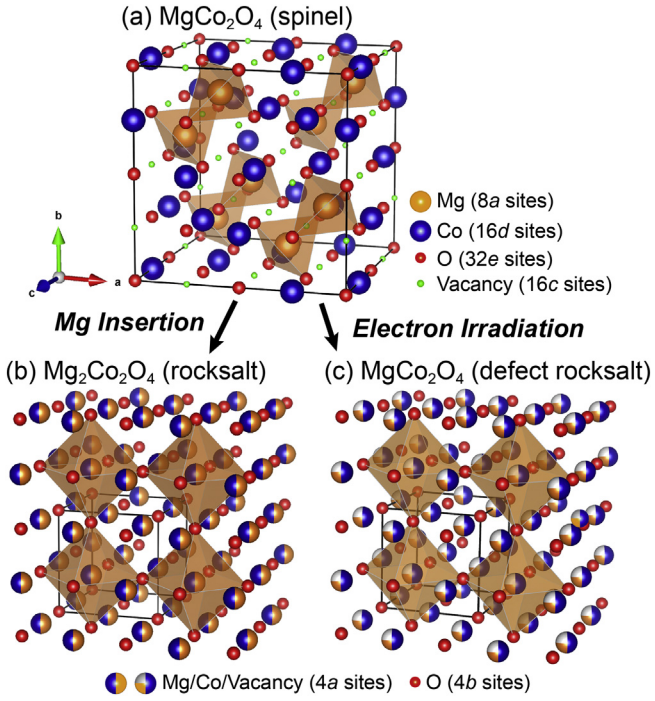

Fig. 1. Perspective views of atomic arrangements in $MgCo_2O_4$ and $Mg_2Co_2O_4$. (a) $MgCo_2O_4$ with the normal spinel structure, (b) $Mg_2Co_2O_4$ with the rocksalt structure where the 4*a* sites, corresponding to the 16*c* and 16*d* sites in the spinel structure with the space group of $Fd\bar{3}m$, are occupied evenly by Mg and Co atoms. (c) $MgCo_2O_4$ with a defect rocksalt structure where a quarter and a half of the 4*a* sites are occupied by Mg and Co atoms, respectively, while the other quarter by vacancies. Unit cells are indicated by black lines.

although no direct evidence of the feasibility of the push-out process has been provided yet.

In the present study, we show in-situ phase change observation of $MgCo_2O_4$ from the spinel structure to a defect rocksalt structure under irradiation of electron beam in a scanning transmission electron microscope (STEM), which elucidates that the Mg cation migration between the tetrahedral (8*a*) and the octahedral (16*c*) sites takes place in a viable manner. This is also examined based on the first-principles calculations of Mg cation migration between the two sites.

Spinel oxide was synthesized by the inverse co-precipitation method [13]. Aqueous metallic nitrate salt solution (0.2 L, 0.080 M Mg (II), 0.160 M Co(II)) was prepared by dissolving $Mg(NO_3)_2{\cdot}6H_2O$ and $CO(NO_3)_2{\cdot}nH_2O$ in deionized water. A sodium carbonate solution (0.4 L, 0.350 M Na_2CO_3) for pH control and precipitation was also prepared. These solutions were heated to 70 °C under vigorous stirring (500 rpm). The metallic nitrate salt solutions were added dropwise into the sodium carbonate precipitation solution. The resulting suspensions were stirred at 70 °C for 30 min and then filtered. The filtered precipitates (precursors) were rinsed with deionized water (600 cm^3) at 70 °C to remove completely Na-containing by-products, and dried in vacuum for 12 h at 110 °C. The precursors were followed by calcination in air at 350 °C for 2 h. A copper-mesh grid covered by a thin perforated carbon film was dipped in approximately 50 mg of the synthesized spinel powder and excess powder was removed from the grid. High-resolution STEM imaging was made with a spherical-aberration-corrected JEOL JEM-ARM200F STEM operated at 200 kV. The probe convergence angle and the inner/outer detector angles for high-angle annular dark-field (HAADF) imaging were 22 and 90–370 mrad, respectively. STEM image simulations were performed with the *WinHREM* software package [14]. To complement the experimental findings, ab initio calculations were performed by using the projector augmented-wave (PAW) method [15] as implemented in the Vienna ab initio simulation package (VASP) [16]. We adopted Perdew-Burke-Ernzerhof generalized gradient approximation to density functional theory [17]. Wave functions were expanded using a plane-wave basis set with a cutoff energy of 520 eV. Appropriate *k*-points were employed by testing the convergence of total energies. The lattice constants and internal atomic positions were fully optimized in all calculations until the residual forces converged to less than 0.01 eV/Å. The nudged elastic band (NEB) method [18], regarded as an efficient algorithm for clarifying the diffusion mechanism and computing activation energies in intercalation electrode materials [12,19], was employed in combination with first-principles calculations for a $Mg_7Co_{16}O_{32}$ ($2 \times 2 \times 2$) normal spinel cell containing one Mg vacancy.

Since we noticed that $MgCo_2O_4$ particles are largely prone to electron irradiation damage as soon as we began STEM observation, we searched for $MgCo_2O_4$ particles with a low-index zone axis at a relatively low magnification as well as at a fast scan rate in order to minimize the effect of electron beam irradiation. Prior to slow scan-rate recording, focusing was done on an uninterested particle in the vicinity of the interested particle in a zone-axis orientation to minimize the irradiation effect on the interested particle. Fig. 2(a) shows a HAADF-STEM image of an as-synthesized $MgCo_2O_4$ particle taken along the [110] direction at a slow scan rate for the first time. Due to the irradiation effect, the HAADF-STEM image of the same $MgCo_2O_4$ particle taken at a slow scan rate for the second time (Fig. 2(h)) is significantly dissimilar to that taken at the first slow scan (Fig. 2(a)). A part of the first shot image indicated by dashed yellow line in Fig. 2(a) is enlarged as shown in Fig. 2(b). A rhombus-shaped pattern of bright contrast indicated by dashed cyan line is deserved to be noticed; the bright and less bright spots, alternately arranged along the edges of the rhombus, reflect the difference in the number density of Co/Mg cations at the 16*d* sites when viewed along the [110] direction since the HAADF contrast is approximately proportional to square of average atomic number in the atomic column (so-called *Z*-contrast imaging) [20]. It is noticed that the contrast of the atomic columns inside the rhombus indicated by dashed circles, corresponding to the 8*a* sites, are brighter in the experimental image (Fig. 2(b)) than that in the calculated image based on the normal spinel structure (Fig. 2(c)), where the 8*a* sites are occupied exclusively by Mg cations while the 16*d* sites exclusively by Co cations (Fig. 2(d)). This suggests that not only Mg cations but also Co cations with the larger atomic number occupy the 8*a* sites. In fact, the experimental image (Fig. 2(b)) well matches the calculated image based on the disordered spinel structure (Fig. 2(e)) of $MgCo_2O_4$ previously determined by the Rietveld analysis [13], in which the 8*a* and 16*d* sites are occupied by both Mg and Co cations (Fig. 2(f)).

However, the HAADF-STEM image of the same $MgCo_2O_4$ particle taken at a slow scan rate for the second time shown in Fig. 2(h) no longer matches the calculated image based on the disordered spinel structure (Fig. 2(e)), indicating that the spinel structure is lost by electron irradiation. The contrast of the atomic columns corresponding to the 8*a* sites in the disordered spinel structure disappeared. Instead, the contrast at the midpoint of the 8*a* sites is bright, which means that the Mg/Co cations at the 8*a* tetrahedral sites migrate to the vacant 16*c* octahedral sites under the electron irradiation. However, the HAADF-STEM image (Fig. 2(i)) calculated for a defect spinel structure, where half the 16*c* sites are occupied by Mg/Co while the 16*d* sites are fully occupied by Co/Mg (Fig. 2(j)), does not match the experimental image (Fig. 2(h)) in the respect that the apparent unit cell of the irradiated $MgCo_2O_4$ particle is half that of the defect spinel structure. It is considered that the crystal structure of the irradiated $MgCo_2O_4$ particle possesses a higher symmetry than the spinel structure owing to an equivalent occupation behavior at the 16*c* and 16*d* sites, which indicates the significant entropy increase as discussed below. When the 16*c* and 16*d* sites are not differentiated, the defect spinel structure becomes a defect rocksalt structure without cation ordering (Fig. 1(c)) because the 16*c* and 16*d* sites in the (disordered) spinel structure correspond to the 4*a* sites in the (defect) rocksalt structure. In the defect rocksalt structure, three quarters of the 4*a* sites are occupied by Mg and Co

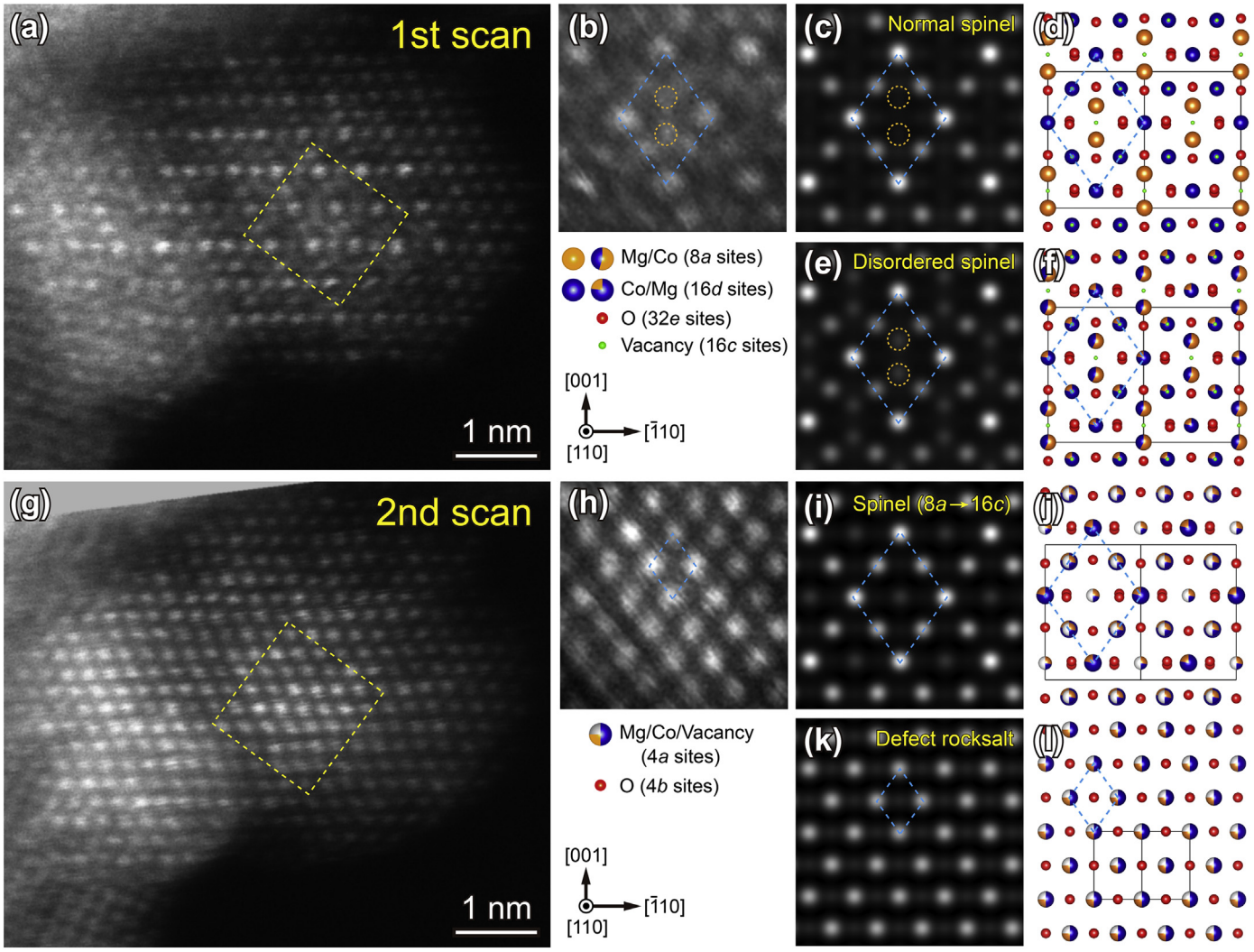

Fig. 2. HAADF-STEM images of an as-synthesized $MgCo_2O_4$ particle. Taken along the [110] direction at the (a) first and (g) second slow scan. (b,h) Maginified and rorated HAADF-STEM images of areas indicated by dashed rectangle in (a) and (g). (c,e,i,k) HAADF-STEM images of $MgCo_2O_4$ with the [110] incidence calculated for (d,f,j,l) four atomic structural models with (c, d) the normal spinel structure, (e,f) the disordered spinel structure previously refined by Rietveld analysis [13], (i,j) a defect spinel structure where half the 16*c* sites are occupied by Mg/Co while the 16*d* sites are fully occupied by Co/Mg, and (k,l) a defect rocksalt structure where half the 4*a* sites are occupied by Mg and Co atoms while the other half by vacancies.

atoms whereas the other quarter is vacant as shown in Figs. 1(c) and 2 (l). In fact, the HAADF-STEM image calculated for the defect rocksalt structure (Fig. 2(k)) well matches the experimental image (Fig. 2(h)). It is considered that Mg/Co cations at the 8*a* tetrahedral sites in the (disordered) spinel structure migrate to the 16*c* octahedral sites and cation exchange between the 16*c* and 16*d* sites also occurs under electron irradiation to form a defect rocksalt structure. The rocksalt structure did not revert to the spinel structure even after leaving the sample in the STEM without electron dose for several minutes.

The fact that the spinel structure transforms to the defect rocksalt structure via migration of Mg/Co cations from the 8*a* tetrahedral sites to the 16*c* octahedral sites under electron irradiation implies that the energy difference between two configurations of Mg cation located either at the 8*a* or 16*c* sites is small. This is demonstrated by first-principles calculations of total energies of supercells with a normal spinel structure which contain one Mg vacancy at 8*a* site so that the supercell composition is $Mg_7Co_{16}O_{32}$. The total energy of the supercell with Mg cation being located at 16*c* site is indeed higher only by 39 meV than that with Mg cation being located at 8*a* site. What is interesting is that after excited by electron irradiation the crystal structure of $MgCo_2O_4$ transforms to the metastable defect rocksalt structure instead of the stable spinel structure. The small energy difference (39 meV) between the spinel structure with the Mg ions located at the 8*a* sites and the defect rocksalt structure with the Mg ions located at the 16*c* sites can be overturned by taking into consideration the entropy increase attributed to disorder in the partially occupied 16*c* sites as explained in the next paragraph.

Since the 8*a* sites are tetrahedrally connected to one another with the 16*c* sites being the midpoint of the adjacent 8*a* sites as shown in Fig. 3(a), there are two equivalent 16*c* sites around each of 8*a* sites in a primitive unit cell. Given that movement of the 8*a*-site cation to another unit cell cannot occur, as a crude approximation, the increase in the entropy term ($T\Delta S_1$) attributed to disorder in the 16*c* sites is estimated as $T\Delta S_1 = k_BT \ln W = k_BT \ln 2^N \sim 0.69RT$, where k_B, T, W, N and R stand for the Boltzmann constant, absolute temperature, number of configurations, Avogadro constant, and gas constant, respectively. Furthermore, we have to consider the mixing effect in 16*c* and 16*d* sites on the entropy increase, which can be roughly estimated as $T\Delta S_2 = (1/4)k_BT \ln [(4N)!/(3N)!N!)] \sim 0.56RT$. Therefore, the total entropy increase by the local transformation from spinel to rocksalt approximates $1.26RT$. The magnitude of the increase in the entropy term exceeds the energy difference between the two configurations (39 meV) when the temperature T is above 361 K (88 °C). The critical temperature would be much lower if the Mg/Co cation disorder is also taken into

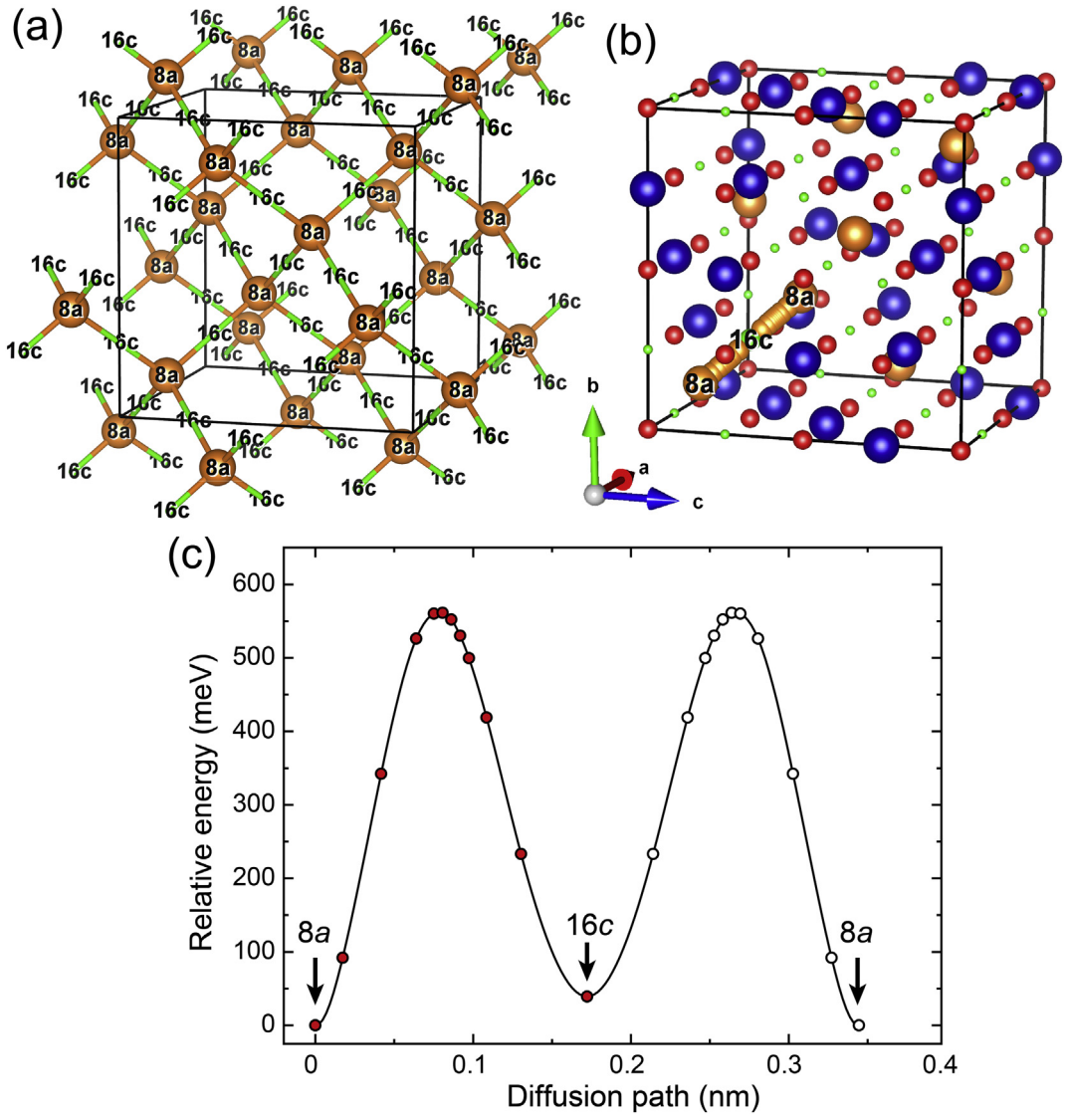

Fig. 3. Arrangement of the 8*a* and 16c sites in the spinel $MgCo_2O_4$ and NEB calculations. (a) Diffusion path of Mg in the spinel structure. The 8*a* sites are tetrahedrally connected to one another with the 16*c* sites being the midpoint of the adjacent 8*a* sites. (b) Calculation supercell with a composition of $Mg_7Co_{16}O_{32}$. The diffusion path of a Mg ion (8*a* – 16*c* – 8*a* sites) are depicted in the figure. (c) Activation energy for the diffusion process of a Mg cation in the $Mg_7Co_{16}O_{32}$ cell estimated by the NEB method. Nodes along the curves indicate the energies of the interpolated images used in the NEB calculations. The right half of the curves is inverted from the left half based on the symmetry of the diffusion process.

consideration. This temperature is reasonably attained by electron irradiation during STEM observation [21] especially due to the low electronic thermal conductivity of the oxide particle supported on a thin carbon film.

The NEB method was employed to determine the saddle point and minimum energy path for migration of Mg cation from 8*a* site to the adjacent vacant 8*a* site through the midpoint 16*c* site as illustrated in Fig. 3 (b). Since the migration path from the 8*a* to 16*c* site is symmetric to that from the 16*c* to 8*a* sites, the minimum energy path was theoretically determined only for half the total path. The activation energy for the Mg migration in the normal spinel $Mg_7Co_{16}O_{32}$ is as high as 561 meV as shown in Fig. 3(c). This activation energy is relatively high compared to that for Li ions in cathode materials of Li-ion batteries (e.g. ~220 meV, $LiFePO_4$ [Ref. [12]]), which might result in sluggish motion of Mg ions in the cathode. Nevertheless, the Mg (de)interaction reactions can take place at 100–150 °C as exemplified by Ref. [13]. Recently, we have elucidated that the activation energy for cation diffusion in cathode materials is significantly reduced by concerted motion of neighboring cations [22]. This cooperative effect among cations together with the small energy difference between two configurations of Mg cation located either at 8*a* or 16*c* sites can explain the relatively feasible Mg (de)interaction reactions in $MgCo_2O_4$.

In summary, we have confirmed the spinel $MgCo_2O_4$ is so prone to electron irradiation damage that the spinel structure readily transforms to a defect rocksalt structure with cation site disorder. This transformation occurs via cation migration from 8*a* to adjacent 16*c* sites. The energy difference between two configurations of Mg cation located either at the 8*a* or 16*c* sites has been confirmed to be small (39 meV) by first-principles calculations. This small energy difference together with the feasible transformation from the spinel structure to a defect rocksalt structure under electron irradiation explains that the Mg insertion into the spinel $MgCo_2O_4$ occurs easily via the intercalation and push-out process of Mg cation so as to show a long plateau region in the potential versus capacity curve on both charge and discharge [13].

This work was supported by the Advanced Low Carbon Technology Research and Development Program - Specially Promoted Research for Innovative Next Generation Batteries(ALCA-SPRING, grant number JPMJAL1301), Grant-in-Aid from the Special Coordination Funds for Promoting Science and Technology commissioned by JST, MEXT of Japan. The authors thank the Center for Computational Materials Science of

the Institute for Materials Research, Tohoku University for the continuous support of the supercomputing facilities (Proposal Nos. 17S0410 and 18S0405).

References

[1] L.A. Dominey, in: D. Aurbach (Ed.), Nonaqueous Electrochemistry. Marcel Dekker, New York 1999, pp. 437–459.
[2] J.M. Tarascon, M. Armand, Nature 414 (2001) 359–367.
[3] M. Matsui, J. Power Sources 196 (2011) 7048–7055.
[4] S. Yagi, T. Ichitsubo, Y. Shirai, S. Yanai, T. Doi, K. Murase, E. Matsubara, J. Mater. Chem. A 2 (2014) 1144–1149.
[5] M. Morita, N. Yoshimoto, S. Yakushiji, M. Ishikawa, Electrochem. Solid-State Lett. 4 (2001) A177–A179.
[6] H.D. Yoo, I. Shterenberg, Y. Gofer, G. Gershinsky, N. Pour, D. Aurbach, Energy Environ. Sci. 6 (2013) 2265–2279.
[7] E. Levi, M.D. Levi, O. Chasid, D. Aurbach, J. Electroceram. 22 (2009) 13–19.
[8] P. Canepa, G.S. Gautam, D.C. Hannah, R. Malik, M. Liu, K.G. Gallagher, K.A. Persson, G. Ceder, Chem. Rev. 117 (2017) 4287–4341.
[9] M.M. Huie, D.C. Bock, E.S. Takeuchi, A.C. Marschilok, K.J. Takeuchi, Coord. Chem. Rev. 287 (2015) 15–27.
[10] D. Aurbach, Z. Lu, A. Schechter, Y. Gofer, H. Gizbar, R. Turgeman, Y. Cohen, M. Moshkovich, E. Levi, Nature 407 (2000) 724–727.
[11] Y.W. Cheng, L.R. Parent, Y.Y. Shao, C.M. Wang, V.L. Sprenkle, G.S. Li, J. Liu, Chem. Mater. 26 (2014) 4904–4907.
[12] Z.Q. Rong, R. Malik, P. Canepa, G.S. Gautam, M. Liu, A. Jain, K. Persson, G. Ceder, Chem. Mater. 27 (2015) 6016–6021.
[13] S. Okamoto, T. Ichitsubo, T. Kawaguchi, Y. Kumagai, F. Oba, S. Yagi, K. Shimokawa, N. Goto, T. Doi, E. Matsubara, Adv. Sci. 2 (2015).
[14] K. Ishizuka, Ultramicroscopy 90 (2002) 71–83.
[15] P.E. Blochl, Phys. Rev. B 50 (1994) 17953–17979.
[16] G. Kresse, J. Furthmuller, Phys. Rev. B 54 (1996) 11169–11186.
[17] J.P. Perdew, K. Burke, M. Ernzerhof, Phys. Rev. Lett. 77 (1996) 3865–3868.
[18] G. Henkelman, B.P. Uberuaga, H. Jonsson, J. Chem. Phys. 113 (2000) 9901–9904.
[19] A. Van Der Ven, J. Bhattacharya, A.A. Belak, Acc. Chem. Res. 46 (2013) 1216–1225.
[20] S.J. Pennycook, L.A. Boatner, Nature 336 (1988) 565–567.
[21] D.D. Thornburg, C.M. Wayman, Phys. Status Solidi A 15 (1973) 449–453.
[22] H.Y. Li, N.L. Okamoto, T. Hatakeyama, Y. Kumagai, F. Oba, T. Ichitsubo, Adv. Energy Mater. 8 (2018).